Methods

Sample preparation

Two Chang'E-5 (CE5) lunar soils (CE5C0100YJFM00103, ~1g, CE5C0400YJFM00406, ~2g) allocated by the China National Space Administration were used in this study. Both of them were scooped by the robotic arm of the CE5 lander and separated into different packages in the ultraclean room at the extraterrestrial sample curation center of the National Astronomical Observatories, Chinese Academy of Sciences. Approximately 240 soil fragments with grain sizes varying from ~100 µm to ~ 1 mm were sieved and hand-picked under a binocular microscope in the ultraclean room at the Institute of Geology and Geophysics, Chinese Academy of Sciences (IGGCAS). Then, about 2/3 of the picked grains were prepared as 8 Sn-Bi metal-alloy mounts following the method of Zhang et al. (2018)[48] and the other 1/3 was mounted in epoxy and prepared as 3 polished thin sections. The polished metal mounts and thin sections were cleaned using ultrapure water and anhydrous ethanol prior to drying at 70 °C in a baking oven overnight. The details of apatite and ilmenite-hosted melt inclusions from 23 CE5 basalt clasts and fragments are summarised in Extended Data Table 1.

Scanning Electron Microscope (SEM) observation

Petrographic observations and elemental mapping were carried out using field emission scanning electron microscopes (FE-SEM) using FEI Nova NanoSEM 450 and Thermofisher Apreo instruments at the IGGCAS, using electron beam currents of 2 to 3.2 nA and an acceleration voltage of 15 kV. Energy dispersive spectroscopy (EDS) X-ray maps were collected for each basaltic clasts to quickly locate P-bearing phases. The phosphates were then observed at higher magnification in back-scattered electron (BSE) images. The modal abundance of apatite from various CE5 basalt clasts were counted by the exposed surface areas (Table S1). The prepared sections were initially coated with Au to identify apatite and melt inclusions for *in situ* NanoSIMS measurement of water content and hydrogen isotopes. Another round of SEM observation was carried out after NanoSIMS measurement to confirm the positions of the NanoSIMS spots.

Electron probe microanalysis

We used a JEOL JXA-8100 electron probe micro-analyzer (EPMA) at the IGGCAS to quantify the major and minor elemental abundances in phosphates, melt inclusions in ilmenite, and associated mafic minerals (i.e. clinopyroxene, olivine, plagioclase, and ilmenite). The samples were coated with carbon. The operating accelerating voltage was 15 kV and the beam current was 20 nA. The EPMA analyses were carried out after the NanoSIMS measurements in order to avoid possible H loss due to bombardment by the electron beam[33]. The EPMA standards were natural albite (Na and Al), bustamite (Mn), diopside (Ca, Si, and Mg), apatite (P), K-feldspar (K), tugtupite (Cl), synthetic fluorite (F), rutile (Ti), Fe_2O_3 (Fe), V_2O_5 (V), NiO (Ni), and Cr_2O_3 (Cr). Sodium, K, F, and Cl were first measured in order to minimise possible loss of volatiles by electron beam irradiation. The detection limits were (1σ) 0.01 wt% for Cl and S, 0.02 wt% for Na, Mg, Al, Cr, K, Si, Mn, Ca and Fe, 0.03 wt% for F, Ba, Ni and Ti, 0.04 wt% for P. A program based on the ZAF procedure was used for data correction. The EPMA data obtained for apatite, melt inclusions in ilmenite, and the coexisting silicates are listed in Table S2.

In situ water abundance and hydrogen isotope analysis

Apatite and melt inclusions

The hydrogen isotopes and water content of apatite and melt inclusions enclosed in ilmenite from the CE5 basaltic clasts were measured with a CAMECA NanoSIMS 50L at IGGCAS. The samples were coated with Au, were loaded in sample holders together with the standards, and were baked overnight at ~60 ºC in the NanoSIMS airlock. The holders were then stored in the NanoSIMS sample chamber to improve the vacuum quality and minimise the H background[49-51]. The vacuum pressure in the analysis chamber was 2.8×10^{-10} to 3.0×10^{-10} mbar during analysis. Each 15 µm × 15 µm analysis area was pre-sputtered for ~ 2 mins with a Cs^+ ion beam current of ~ 2 nA to remove the surface coating and potential contamination. During analysis, the secondary anions $^1H^-$, $^2D^-$, $^{12}C^-$, and $^{16}O^-$ were simultaneously counted by electron multipliers (EMs) and a Faraday cup from the central 3 µm × 3 µm areas using the NanoSIMS blanking technique. A 44 ns dead time was corrected for all EMs, while the EM noise ($<10^{-2}$ cps) was ignored. We used a primary ion beam current of ~0.5 nA for analysis, corresponding to a beam size of ~500 nm in diameter. The charging effect on the samples surface was compensated by an electron-gun during analysis. A chip of the anhydrous San Carlos olivine was used for H background corrections, following the relationship: $H/O_{bg} = (H_{counts} - H_{bg}) / O_{counts}$ and $D/H_{measured} = (1-f) \times D/H_{true} + f \times D/H_{bg}$, where f is the proportion of H emitted from the instrumental background[52]. Here, D/H_{bg} was 3.36 (±0.55)$\times10^{-4}$ and H_{bg} = 7.36 (±1.49) × 10^4 (2SD, N=11, corresponding to H_2O background abundance of 25 ± 8 µg.g^{-1} (2SD)). Corrections for matrix effects and instrumental mass fractionation (IMF) on water abundance (Extended Data Fig. 2) and H isotope determination (Extended Data Fig. 3) were determined by measuring two apatite standards, Durango apatite (H_2O = 0.0478 wt% and δD = -120 ± 5‰) [29, 53] and Kovdor apatite (H_2O = 0.98 ± 0.07 wt.% and δD = -66 ± 21‰)[54], the SWIFT MORB glass (H_2O = 0.258 wt.% and δD = -73 ± 2‰), and two basaltic glasses, 519-4-1 (H_2O = 0.17 wt.%)[49] and 1833-11 (H_2O = 1.2 wt.%)[49] (Table S3). Hydrogen isotopic compositions are given using the delta notation, $\delta D = ((D/H)_{sample}/(D/H)_{SMOW})-1) \times 1000$ ‰, where SMOW is the standard mean ocean water with a D/H ratio of 1.5576×10^{-4}. More technical details can be found in to Hu et al. (2014, 2015)[50, 51]. All data are reported with their 2σ uncertainties that include reproducibility of D/H measurements on the reference materials, uncertainty of H_2O background subtraction, and internal precision on each analysis (Extended Data Tables 2 and 3 and Table S4). The raw measured D/H ratios were corrected for the background, followed by correction for IMF.

Clinopyroxene

The water abundance of clinopyroxene from the CE5 basaltic clasts was measured with the CAMECA NanoSIMS 50L using an identical instrument setup to that described above. We used a higher Cs^+ primary beam current of 7 nA to improve the $^1H^-$ counts on clinopyroxene. Each 25 µm × 25 µm analysis areas was pre-sputtered for ~ 2 mins with the same analytical beam current to remove surface coating and potential contaminations. The secondary ion signals from the central 7 µm × 7 µm areas were counted with 50% blanking of outermost regions. San Carlos olivine (H_2O = 1.4 µg.g^{-1}, ref. [55]) was used for determining instrumental background of H. The analytical results are listed in Extended Data Table 4.

Correction of water abundances and D/H ratios for spallation effects

The measured D/H ratios have also been corrected for the potential effects of spallation by cosmic-ray, using a D production rate of 2.17 × 10^{-12} mol D/g/Ma[56] for melt inclusions and 9.20 × 10^{-13} mol D/g/Ma[57] for apatite. The correction errors induced by D spallation are around 50% on δD and negligible on water content[21]. The cosmic ray exposure (CRE) ages determined for most Apollo samples are less than ~200 Ma[37]. Because no CRE age is yet available for the Chang'E-5 basaltic clasts, we modeled the effects of corrections for CRE ages of 10, 50, 100 and 200 Ma (Extended Data Table 3 and Fig. 4). The corrected δD values for the melt inclusions with low water abundances appear to be over-corrected for CRE ages of 100 and 200 Ma, as indicated by unusually low δD values. We thus decided to correct δD values using a CRE age of 50 Ma, slightly older than that of Apollo lithic fragments (1-24 Ma) [58], for which the corrected δD values of the melt inclusions with low H_2O are comparable to the lowest δD values measured in apatite (~300‰), as apatite crystallization postdated that of ilmenite in which the melt inclusions are hosted.

Degassing modeling

The hydrogen isotope fractionation during volatile loss into a vacuum is given by $\alpha^2 = M1/M2$, where M1 and M2 are the masses of the volatile phase isotopologues. The change of the isotopic composition of H during volatile loss by Rayleigh fractionation is given by $R = R_0 \times f^{(\alpha-1)}$, where R_0 and R are the initial and final D/H ratios for a fraction f of remaining hydrogen[39]. Degassing of H_2 (M1 = 2 for H_2 and M2 = 3 for HD) yields an α value of ~0.8165, and degassing of H_2O (M1 = 18 for H_2O and M2 = 19 for HDO) yields an α value of ~0.9733[39] (Extended Data Fig. 4).

References

48. Zhang, W.F., et al. A novel sample preparation method for ultra-high vacuum (UHV) secondary ion mass spectrometry (SIMS) analysis. *J Anal Atom Spectrom* **33**,1559-1563 (2018).
49. Hauri, E., et al. SIMS analysis of volatiles in silicate glasses 1. Calibration, matrix effects and comparisons with FTIR. *Chem Geol* **183**,99-114 (2002).
50. Hu, S., et al. NanoSIMS analyses of apatite and melt inclusions in the GRV 020090 Martian meteorite: Hydrogen isotope evidence for recent past underground hydrothermal activity on Mars. *Geochim Cosmochim Ac* **140**,321-333 (2014).
51. Hu, S., et al. Measurements of water content and D/H ratio in apatite and silicate glasses using a NanoSIMS 50L. *J Anal Atom Spectrom* **30**,967-978 (2015).
52. Tartese, R., M. Anand, and I.A. Franchi H and Cl isotope characteristics of indigenous and late hydrothermal fluids on the differentiated asteroidal parent body of Grave Nunataks 06128. *Geochim Cosmochim Ac* **266**,529-543 (2019).
53. Greenwood, J.P., et al. Hydrogen isotope evidence for loss of water from Mars through time. *Geophys Res Lett* **35**,L05203 (2008).
54. Nadeau, S.L., S. Epstein, and E. Stolper Hydrogen and carbon abundances and isotopic ratios in apatite from alkaline intrusive complexes, with a focus on carbonatites. *Geochim Cosmochim Ac* **63**,1837-1851 (1999).
55. Zhang, W.F., et al. Optimization of SIMS analytical parameters for water content measurement of olivine. *Surf Interf Anal* **52**,224-233 (2019).
56. Furi, E., E. Deloule, and R. Trappitsch The production rate of cosmogenic deuterium at the Moon's surface. *Earth Planet Sc Lett* **474**,76-82 (2017).
57. Merlivat, L., et al., *Spallation deuterium in rock 70215*, in *Lunar and Planetary Science Conference Proceedings*. 1976. p. 649-658.
58. Das, J.P., S.L. Baldwin, and J.W. Delano 40Ar/39Ar and cosmic ray exposure ages of plagioclase-rich lithic fragments from Apollo 17 regolith, 78461. *Earth Planet Space* **68**,11 (2016).
59. Guggisberg, S., et al. Classification of the Apollo-11 mare basalts according to/Ar-39/-/Ar-40/ages and petrological properties. Lunar and Planetary Science Conference Proceedings **10**,1-39 (1979).
60. Papanastassiou, D., G. Wasserburg, and D. Burnett Rb-Sr ages of lunar rocks from the Sea of Tranquillity. *Earth Planet Sc Lett* **8**,1-19 (1970).
61. Nyquist, L., et al. The SR and Nd isotopic record of Apollo 12 basalts-Implications for lunar geochemical evolution. Lunar and Planetary Science Conference Proceedings **10**,77-114 (1979).

62. Papanastassiou, D. and G. Wasserburg RbSr ages of igneous rocks from the Apollo 14 mission and the age of the Fra Mauro formation. *Earth Planet Sc Lett* **12**,36-48 (1971).
63. Saal, A.E., et al. Volatile content of lunar volcanic glasses and the presence of water in the Moon's interior. *Nature* **454**,192-5 (2008).
64. Snyder, G., et al. Volcanism in the Hadley-Apennine region of the Moon: Geochronology, Nd-Sr isotopic systematics, and depths of melting. Lunar and Planetary Science Conference 1141 (1998).
65. Husain, L. 40Ar-39Ar chronology and cosmic ray exposure ages of the Apollo 15 samples. *Journal of Geophysical Research* **79**,2588-2606 (1974).
66. Tatsumoto, M., W.R. Premo, and D.M. Unruh Origin of Lead from Green Glass of Apollo-15426 - a Search for Primitive Lunar Lead. *J Geophys Res-Solid* **92**,E361-E371 (1987).
67. York, D., W.J. Kenyon, and R.J. Doyle 40Ar-39Ar ages of Apollo 14 and 15 samples. Lunar and Planetary Science Conference Proceedings **3**,1613 (1972).
68. Saito, K. and E. Alexander 40AR-39AR Studies of Lunar Soil 74001. Lunar and Planetary Science Conference **10**,1049-1051 (1979).
69. Furi, E., et al. New evidence for chondritic lunar water from combined D/H and noble gas analyses of single Apollo 17 volcanic glasses. *Icarus* **229**,109-120 (2014).
70. Tera, F. and G. Wasserburg Lunar ball games and other sports. Lunar and Planetary Science Conference **7**,(1976).
71. Tera, F., D.A. Papanastassiou, and G.J. Wasserburg Isotopic Evidence for a Terminal Lunar Cataclysm. *Earth Planet Sc Lett* **22**,1-21 (1974).
72. Fernandes, V.A., R. Burgess, and A. Morris 40Ar - 39Ar age determinations of lunar basalt meteorites Asuka 881757, Yamato 793169, Miller Range 05035, La Paz Icefield 02205, Northwest Africa 479, and basaltic breccia Elephant Moraine 96008. *Meteorit Planet Sci* **44**,805-821 (2009).
73. Anand, M., et al. Petrology and geochemistry of LaPaz Icefield 02205: A new unique low-Ti mare-basalt meteorite. *Geochim Cosmochim Ac* **70**,246-264 (2006).
74. Yang, W. and Y. Lin New lunar samples returned by Chang'E-5: Opportunities for new discoveries and international collaboration. *The Innovation* **2**,100070 (2021).

Data availablility

All geochemical data generated in this study are included in Extended Data Table 1-4 and in Supplementary Table S1-S5.

Code availability

No code is used in this study.

Acknowledgements

We thank David Chew for providing Durango and Kovdor apatite, Erik Hauri for providing basaltic glass 519-4-1 and 1833-11, Robert Francis for providing SWIFT MORB glass, Ross Mitchell, Xian-Hua Li, and Fu-Yuan Wu for constructive comments, Yi Chen and Lihui Jia for the assistance on EPMA measurement, Hongxia Ma and Danping Zhang for hand picking the CE5 soil fragments, and Jiangyan Yuan and Xu Tang for the assistance on SEM observation. This study was funded by the Strategic Priority Research Program of Chinese Academy of Sciences (XDB 41000000), the key research program of Chinese Academy of Sciences (ZDBS-SSW-JSC007-15), and the key research program of the Institute of Geology and Geophysics, Chinese Academy of Sciences (IGGCAS-202101 and 201904), the National Natural Science Foundation of China (41973062), and Pre-research project on Civil Aerospace Technologies by CNSA (D020201 and D020203). MA and RT acknowledge funding from the UK Science and Technology Facilities Council (grant #ST/P000657/1 and # ST/P005225/1, resp.). The CE5 samples were allocated by the China National Space Administration.

Author contributions

S. H., Y. L., and H. H. designed this research. J. J., H. H., Y. Y., J. L., L. G., Q. G., and S. H. prepared the sample and characterized the petrography and mineral chemistry of CE5 basalts. H. H., J. H., R. L., J. J., and S. H conducted the NanoSIMS measurements. S. H., Y. L., H.H., J. J., H. H, M. A., R. T., and H. H. wrote the manuscript. All authors contributed to the preparation of the manuscript.

Competing interests: The authors declare no competing interests.

Additional information

Extended Data Table 1 | The Chang'E-5 basalt clasts

Clast No.	Mount form*	Size (mm)	Texture	Apatite (μm)	Melt inclusion (μm)
CE5C0100YJFM00406					
406-010,001	Sn-Bi alloy	0.87×0.39	Poikilitic	~3	
406-010,019	Sn-Bi alloy	0.58×0.35	Poikilitic	~3	
406-010,023	Sn-Bi alloy	0.79×0.57	Poikilitic	10	17×11
406-011,003	Sn-Bi alloy	0.89×0.59	Equigranular	5 to 10	
406-011,007	Sn-Bi alloy	0.70×0.30	Poikilitic	3 to 5	
406-012,004	Sn-Bi alloy	0.89×0.58	Subophitic	3 to 5	
406-012,009	Sn-Bi alloy	0.69×0.611	Fragment	~3	<50×17
406-014,001	PTS	0.39×0.18	Fragment	<10	
406-014,003	PTS	0.80×0.71	Subophitic	~5	
406-015,001	PTS	1.17×0.72	Fragment	10	
406-015,014	PTS	0.25×0.15	Equigranular	10	
406-015,045	PTS	0.51×0.39	Subophitic	3 to 5	19×7
406-015,046	PTS	0.67×0.29	Subophitic	3 to 5	6×4
406-015,048	PTS	0.59×0.36	Subophitic	5 to 10	
406-015,059	PTS	0.68×0.30	Poikilitic	3 to 5	
CE5C0100YJFM00103					
103-017,001	Sn-Bi alloy	1.05×0.42	Poikilitic	~3	55×40
103-017,010	Sn-Bi alloy	0.45×0.27	Equigranular	~5	
103-017,011	Sn-Bi alloy	0.64×0.44	Equigranular	~5	
103-015,013	Sn-Bi alloy	0.54×0.52	Poikilitic	~5	10×7
103-020,004	PTS	0.25×0.24	Fragment	10	
103-020,013	PTS	0.37×0.21	Fragment		25×13
103-020,018	PTS	0.41×0.30	Fragment	<3	17×4
103-020,021	PTS	0.39×0.23	Poikilitic	5 to 10	

*Sn-Bi alloy mount, PTS-polished thin section.

Extended Data Table 2 | Water abundance and hydrogen isotopes of CE5 apatite

		CRE age = 0 Ma				CRE age = 50 Ma*	
File Name	**Clast No.**	**H_2O μg.g^{-1}**	**2σ μg.g^{-1}**	**δD ‰**	**2 σ ‰**	**H_2O μg.g^{-1}**	**δD ‰**
010-001Ap-1	406-010,001	2205	91	382	64	2205	381
010-001Ap-2	406-010,001	1850	79	461	67	1850	460
010-019Ap-1	406-010,019	2418	109	422	65	2418	421
010-019Ap-2	406-010,019	2153	96	363	64	2153	362
010-023Ap-1	406-010,023	176	17	722	169	176	708
010-023Ap-2	406-010,023	236	19	426	159	235	416
010-023Ap-3	406-010,023	110	13	440	210	110	418
011-003Ap-1	406-011,003	2936	119	464	62	2936	463
011-007Ap-1	406-011,007	1626	73	276	69	1626	275
012-004Ap-1	406-012,004	2595	108	382	70	2595	381
012-004Ap-2	406-012,004	2755	110	456	60	2755	455
012-009Ap-1	406-012,009	1936	87	551	67	1936	550
014-001Ap-1	406-014,001	4363	187	329	57	4363	329
014-001Ap-2	406-014,001	1841	82	368	67	1841	367
014-003Ap-1	406-014,003	4856	217	376	66	4856	376
015-001Ap-1	406-015,001	1137	53	368	80	1137	366
015-001Ap-2	406-015,001	1167	56	512	80	1166	510
015-001Ap-3	406-015,001	939	46	566	84	939	563
015-014Ap-1	406-015,014	1717	74	931	63	1717	929
015-014Ap-2	406-015,014	1652	71	814	64	1651	812
015-014Ap-3	406-015,014	791	40	723	83	791	720
015-014Ap-4	406-015,014	1461	64	834	69	1461	832
015-014Ap-5	406-015,014	1983	88	857	61	1983	856
015-014Ap-6	406-015,014	1214	54	878	70	1213	877
015-014Ap-7	406-015,014	1139	52	861	70	1138	859
015-014Ap-8	406-015,014	1312	59	1024	71	1312	1022
015-014Ap-9	406-015,014	1217	54	826	70	1217	824
015-014Ap-10	406-015,014	1516	67	886	65	1516	884
015-014Ap-11	406-015,014	2361	98	930	59	2361	929
015-014Ap-12	406-015,014	952	45	703	78	952	700
015-046Ap-1	406-015,046	1574	69	368	75	1574	367
015-048Ap-1	406-015,048	1127	65	609	77	1127	607
015-059Ap-1	406-015,059	1166	57	754	77	1166	752
017-010Ap-1	103-017,010	1606	75	321	73	1606	320
017-011Ap-1	103-017,011	1714	80	412	68	1714	411
017-011Ap-2	103-017,011	2322	96	479	65	2322	478
017-013Ap-1	103-017,013	1920	87	562	66	1920	561
020-018Ap-1	103-020,018	555	31	564	98	555	560
020-021Ap-1	103-020,021	3681	169	511	55	3681	511
020-021Ap-2	103-020,021	3077	134	563	58	3077	562
020-004Ap-1	103-020,004	1807	82	451	70	1807	450
020-004Ap-2	103-020,004	2164	91	519	64	2164	518
020-004Ap-3	103-020,004	2049	93	509	64	2049	508

*D production rate of 9.20×10^{-13} mol D/g/Ma[57] was used for cosmogenic spallation effects. CRE age: cosmic ray exposure age.

Extended Data Table 3 | Water abundance and hydrogen isotopes of CE5 ilmenite-hosted melt inclusions

		CRE age = 0 Ma				CRE age = 50 Ma*	
File Name	**Clast No.**	**H_2O μg.g^{-1}**	**2σ μg.g^{-1}**	**δD ‰**	**2σ ‰**	**H_2O μg.g^{-1}**	**δD ‰**
010-023MI-1	406-010,023	26	6	411	349	26	177
012-009MI-1	406-012,009	89	16	-147	322	89	-216
015-045MI-1	406-015,045	661	37	281	113	661	271
015-046MI-1	406-015,046	174	18	581	161	174	547
017-013MI-1	406-017,013	93	15	933	224	93	869
017-001MI-1	406-017,001	27	6	243	339	27	18
017-001MI-2	406-017,001	13	4	669	390	13	202
020-013MI-1	103-020,013	367	29	-313	164	367	-330
020-013MI-2	103-020,013	281	23	-310	182	281	-332
020-018MI-1	103-020,018	114	11	-180	213	114	-234
020-018MI-2	103-020,018	154	13	-94	180	154	-133

*D production rate of 2.17×10^{-12} mol D/g/Ma[56] was used for correction of comogenic spallation effects. CRE age: cosmic ray exposure age.

Extended Data Table 4 | H/O ratios of CE5 clinopyroxene and reference San Carlos olivine measured by NanoSIMS 50L

Clast No.	Grain#	$^{1}H_{Counts}$	$^{16}O_{Counts}$	$^{1}H/^{16}O$	Err Mean	Poisson
Standard	SanCarlosOl-1	1.39E+05	5.40482E+010	2.58E-06	8.500E-001	2.68E-01
Standard	SanCarlosOl-2	1.19E+05	4.64532E+010	2.56E-06	1.150E+000	2.90E-01
Standard	SanCarlosOl-3	1.12E+05	4.12918E+010	2.71E-06	8.360E-001	2.99E-01
Standard	SanCarlosOl-4	6.21E+04	4.62124E+010	1.34E-06	7.490E-001	4.01E-01
Avg.				*2.30E-6*		
406-016,017	016-017CPX-1	5.11E+04	4.94974E+010	1.03E-06	8.820E-001	4.42E-01
406-016,017	016-017CPX-2	5.78E+04	5.46378E+010	1.06E-06	8.260E-001	4.16E-01
406-012,009	012-009CPX-1	3.69E+04	6.13187E+010	6.02E-07	7.830E-001	5.20E-01
103-017,010	017-010CPX-1	5.07E+04	5.30020E+010	9.56E-07	1.170E+000	4.44E-01
406-010,023	010-023CPX-1	4.61E+04	6.48510E+010	7.11E-07	7.980E-001	4.66E-01
103-020,013	020-013CPX-1	6.37E+04	5.12381E+010	1.24E-06	7.200E-001	3.96E-01
406-016,013	020-013CPX-2	5.85E+04	5.46135E+010	1.07E-06	8.240E-001	4.13E-01
406-016,011	016-011CPX-1	7.20E+04	5.62715E+010	1.28E-06	5.990E-001	3.73E-01
103-018,001	018-001CPX-1	4.44E+04	5.91575E+010	7.50E-07	6.450E-001	4.75E-01
103-018,005	018-001CPX-2	4.74E+04	6.10594E+010	7.76E-07	5.610E-001	4.60E-01
406-016,005	016-005CPX-1	4.79E+04	7.38569E+010	6.49E-07	5.150E-001	4.57E-01
103-020,001	020-001CPX-1	7.99E+04	6.41275E+010	1.25E-06	4.660E-001	3.54E-01
103-020,018	020-018CPX-1	6.81E+04	6.03355E+010	1.13E-06	5.150E-001	3.83E-01
103-020,018	020-018CPX-2	6.58E+04	5.82048E+010	1.13E-06	8.080E-001	3.90E-01
406-010,023	010-023CPX-2	4.01E+04	6.86893E+010	5.84E-07	6.320E-001	4.99E-01
406-010,019	010-019CPX-1	4.60E+04	7.55480E+010	6.09E-07	6.740E-001	4.66E-01
406-010,019	010-019CPX-2	3.72E+04	6.61077E+010	5.62E-07	6.840E-001	5.19E-01
406-010,019	010-019CPX-3	3.72E+04	6.90618E+010	5.39E-07	7.200E-001	5.18E-01
Avg.				*8.85E-7*		

Extended Data Table 5 | Summary of the water abundances estimated for the lunar mantle source regions of basaltic products formed between ca. 4-2 Ga.

Sample name	Age (Ga)*	References	Phase#	H_2O_{min} (μg.g^{-1})	H_2O_{max} (μg.g^{-1})	References
10020	3.7	59	MI	3	60	11
10044	3.71	60	Ap	2.12	3.12	29, 33
10058	3.63	60	Ap	9	28	15
10058	3.63	60	MI	3	60	11
12002	3.36	60	MI	3	3	11
12004	3.36	60	MI	3	3	11
12008	3.36	60	MI	3	3	11
12018	ND		MI	25	160	11, 35
12020	3.36	60	MI	3	3	11
12039	3.19	61	Ap	2.4	15.12	15, 28, 29, 32
12040	3.36	60	MI	3	3	11
12064	3.18	62	Ap	2	7	25, 33
14053	3.96	62	Ap	1.42	26	29, 34, 63
14072	3.99	6	MI	3	60	11
15016	3.34	64	MI	3	60	11
15058	3.36	65	Ap	1	4	14, 15
15427	3.41	66	GB	5.2	14.9	63
15555	3.31	67	Ap	10	30	15
74002	3.66	68	GB	4	92	69
74220	3.48	70	MI	9	130	8, 25
74220	3.48	70	MI	133	292	22
74220	3.48	70	MI	88	124	9
74235	3.48	70	MI	84	84	10
75055	3.77	71	Ap	4	13	28, 29, 32
NWA 2977	2.86	5	Ap	7.2	17	14
MIL 05035	3.85	72	Ap	8	26	15
LAP 04841	3.0	73	Ap	53	166	15
CE5	2.03	3	MI	2	6	This study

*ND=No data.

#MI-Melt inclusions, Ap-Apatite, GB-Glass bead. They were used for estimating water abundance in the lunar mantle.

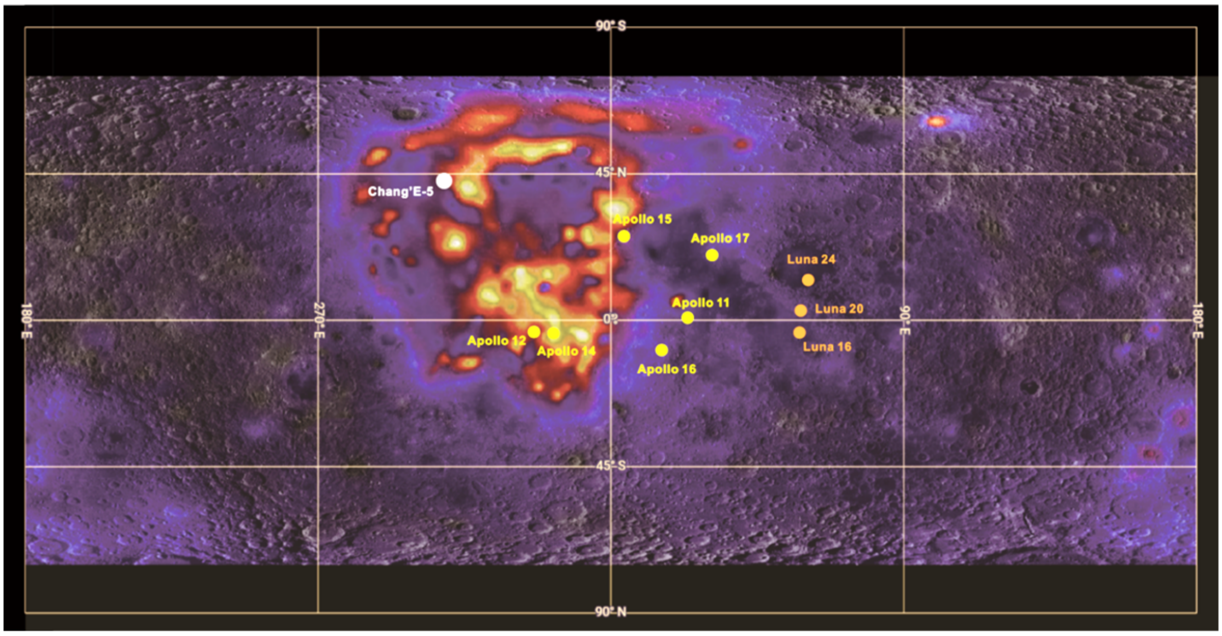

Extended Data Fig. 1 | Location of CE5 samples on the Moon. Chang'E-5 landed in the northwestern Oceanus Procellarum KREEP-rich terrain (represented by Th abundance) on December 17th, 2020[31, 74], far from the landing sites of Apollo and Luna missions. The map (LROC WAC Basemap) and the overlapping Th distribution (Lunar Prospector) are from https://quickmap.lroc.asu.edu/.

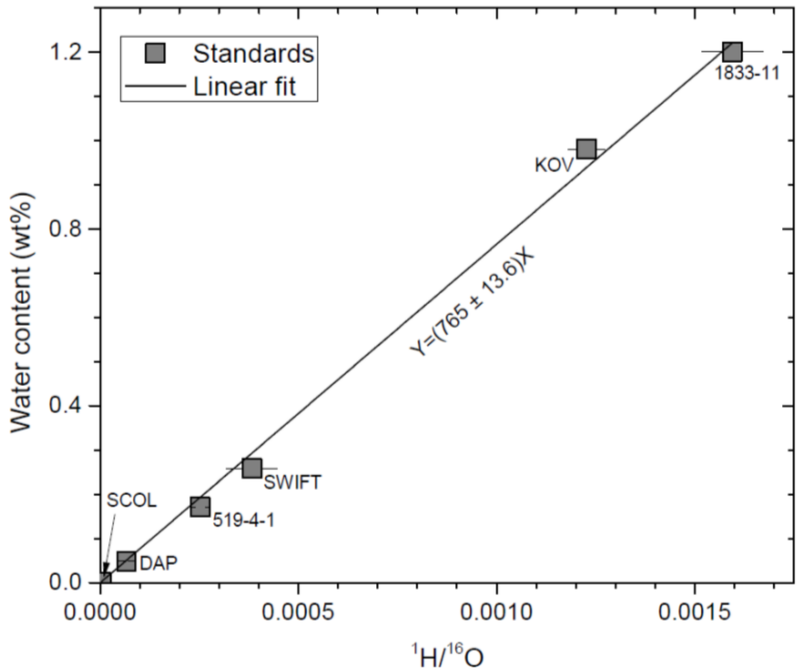

Extended Data Fig. 2 | The water content calibration line established on standards. KOV: Kovdor apatite, DAP: Durango apatite, SWIFT: SWIFT MORB glass, 519-4-1: basaltic glass, 1833-11: basaltic glass, SCOL: San Carlos olivine. The data sets are listed in Table S3. The analytical uncertainty is 0.6% (2σ).

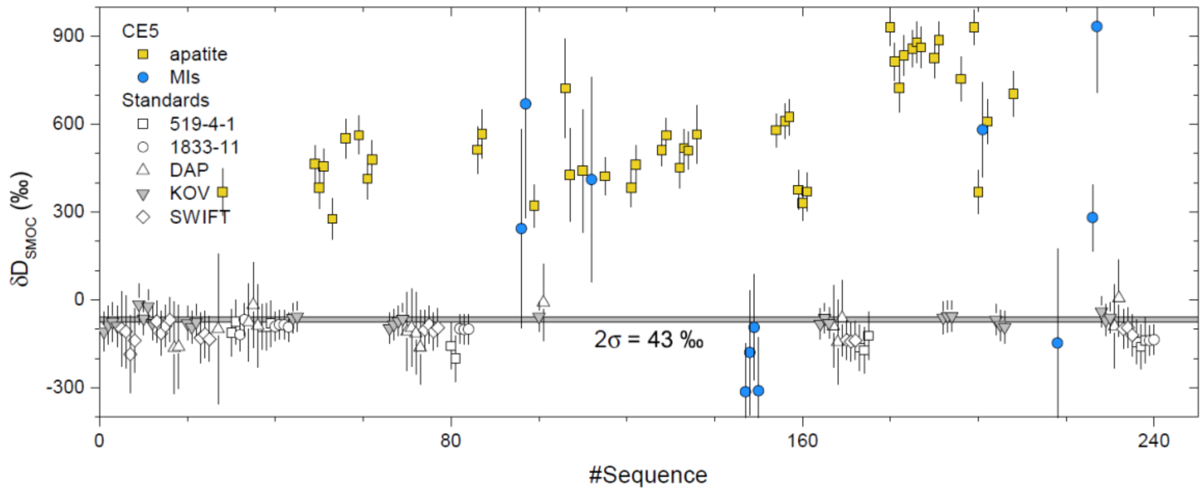

Extended Data Fig. 3 | Reproducibility of hydrogen isotope analysis of the standards and the CE5 apatite and ilmenite-hosted melt inclusions over the analytical session. The reproducibility of δD analysis throughout the whole analytical sessions was ±43 ‰ (2σ), estimated on the Kovdor apatite standard. The average δD values measured for the SWIFT MORB glass and Durango apatite are -113 ± 109 ‰ and -92 ± 210 ‰, respectively, consistent with their recommended values[29, 53] within analytical errors. The average δD values measured for the basaltic glass standards 1833-11 and 519-4-1 are -101 ± 86 ‰ and -132 ± 158 ‰, respectively. All analytical data are listed in Extended Data Tables 3 and 4 and Table S3.

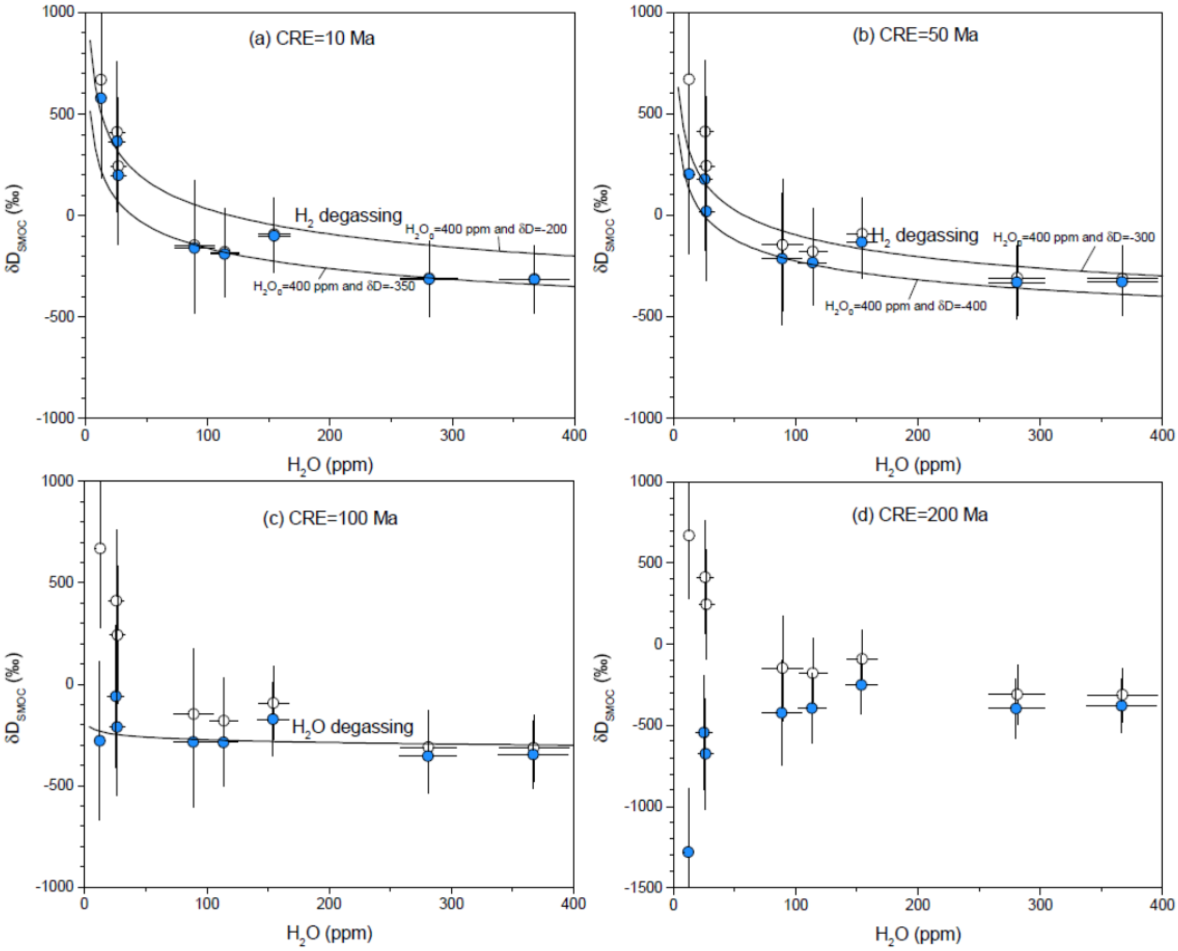

Extended Data Fig. 4 | Spallation correction modeling for ilmenite-hosted melt inclusions. A cosmogenic D production rate of 2.17×10^{-12} mol D/g/Ma[56] was used for melt inclusions glasses. (a) Cosmic-ray exposure (CRE) age = 10 Ma. (b) CRE = 50 Ma. (c) CRE =100 Ma. (d) CRE = 200 Ma. Open circles correspond to measured data, and blue filled circles correspond to CRE-corrected data (Extended Data Table 4 and Table S4). Modeled degassing curves have been calculated assuming Rayleigh fractionation into a vacuum, using masses of 2.016 and 3.022, and a fractionation factor of $(2.016/3.022)^{1/2}$ for H_2, and masses of 18.015 and 19.021, corresponding to a fractionation factor of $(18.015/19.021)^{1/2}$ for H_2O, following the procedure of ref. [39] (see text for details).